Title
Measuring pH Changes Inside a Bipolar Membrane Junction

Journal
ACS Energy Letters

ISSN
2380-8195

Authors
Hou, Shujin
Stovall, T Nathan
Weber, Adam Z
et al.

Publication Date
2026

DOI
10.1021/acsenergylett.5c03710

Measuring pH changes inside a bipolar membrane junction

Shujin Hou[1,2,3], T. Nathan Stovall[1,2], Adam Z. Weber[2], Shannon W. Boettcher[1,2,3,*]

[1]*Department of Chemical & Biomolecular Engineering and Department of Chemistry, University of California, Berkeley, CA 94720, USA*

[2]*Energy Storage and Distributed Resources Division, Lawrence Berkeley National Laboratory, Berkeley, CA 94720, USA*

[3]*Oregon Center for Electrochemistry, Department of Chemistry and Biochemistry, University of Oregon, Eugene, Oregon 97403, USA.*

ABSTRACT

The local pH environment within bipolar membrane (BPM) junctions is complex and not well understood, yet it is important to control for advancing performance BPM-based electrochemical systems. We report a voltammetric strategy using an ultrathin Ni mesh pH probe to spatially resolve pH changes in the BPM junction during model BPM electrolyzer operation. Under reverse bias, we observe depletion of OH^- at the anion-exchange layer (AEL) interface, with a degree diminishing with increasing distance from the AEL. These gradients correlate with current-dependent water dissociation (WD) and are modulated by the electric field and the surface charge state of the catalyst. By correlating spatial pH profiles with the surface-charging behavior of WD catalysts, we explore a mechanism of catalyst-mediated H^+ and OH^- transfer facilitated by hydrogen-bonding networks. These findings highlight the role of local chemistry and electrostatics in BPM performance and offer new methods to probe and engineer catalytic junctions in electrochemical energy devices.

Electrochemical technologies are central to energy storage, conversion, chemical manufacturing, and separation processes.[1-4] A key challenge in engineering electrochemical systems lies in the control of ionic species generation and selective transport.[5-7] Bipolar membranes (BPMs) use ionomer heterojunctions to control ionic current flow and engineer local-pH microenvironments.[8, 9] BPMs consist of an ionomer anion-exchange layer (AEL) and a cation-exchange layer (CEL), laminated together to form a bilayer ionic heterojunction, analogous to semiconductor *pn* electronic junctions.[10] BPMs have been used in electrodialysis,[11, 12] fuel cells,[13] and electrolysis of water and carbon dioxide.[3, 8, 14] The integration of BPMs in electrolyzers enables the simultaneous operation of cathodic and anodic processes under acidic and alkaline conditions, respectively. These different local pH environments at the electrodes enhances water oxidation and reduction reactions, and opens pathways for performance optimization that could reduce or eliminate reliance on precious-metal catalysts.[9, 15, 16]

Engineering BPMs for these technologies requires precise control over the underlying ion transport and charge-transfer processes.[17] When a sufficient bias voltage is applied to the BPM, water dissociation (WD) occurs at the interface between the AEL and CEL ($H_2O \rightarrow H^+ + OH^-$).[10] The generated H^+ ions are driven through the CEL, while OH^- ions through the AEL. Current commercial BPMs necessitate significant overpotentials to facilitate effective WD.[3] To reduce the WD overpotential (η_{wd}) catalysts such as metal oxides/hydroxides, conducting polymers, and graphene-oxide nanosheets have been incorporated within BPM junctions.[10, 18, 19] Despite practical advances lowering η_{wd}, the underlying mechanisms of WD, and the coupled ion-transport processes at/in the BPM junction remain poorly understood, especially regarding the exact role of electric fields and local pH in catalyst layers with diverse surface, electronic and dielectric properties.[20-22] Further, the structure of the water network at the junction and the ion transport pathways on, in, or near catalyst surfaces are unclear.[23-25]

WD under reverse bias is central to BPM performance, creating the H^+ and OH^- ions for catalytic reactions at the cathode and anode. In one hypothesized mechanism, the transmembrane electric field is focused at catalyst surfaces and lowers the entropic barrier associated with interfacial proton transfer, leading to increased WD rates with voltage bias.[10, 20, 26] Metal-oxide surfaces in aqueous environments typically feature acid-base sites such as terminal M–OH or bridging M–O–M groups. The intrinsic proton-transfer kinetics and surface electrostatic gradients that arise from

fixed surface charges (via protonation or deprotonation) are significantly influenced by the oxide's acid-base chemistry.[3, 26, 27] Previous studies proposed that optimal WD catalyst performance occurs when the surface's point of zero charge (PZC) matches the local pH conditions, although the precise reasons for this remain unclear.[3] Regardless, understanding the spatial pH profiles within the junction, particularly before, during, and after BPM operation, would be useful in elucidating the WD mechanism. Given the sub-micrometer thickness of WD catalyst layers, conventional pH measurement techniques are impractical. With the development of local pH measurement techniques in the fields of biology and (electro)chemistry, microscopic pH can be also measured by micro/nanoprobe or spectroscopic methods.[28-31] Common electrochemical methods for evaluating pH include potentiometric, voltammetric, conductimetric, capacitive, and resistive techniques, all of which leverage the sensitivity of metals, metal oxides, or conductive polymers to interfacial H^+ or OH^- ions.[28] Voltammetric pH sensors, in particular, offer sufficient temporal and spatial resolution, making them useful for studying electrode interfaces and cellular environments.[32-34]

Voltammetric pH sensors rely on pH-dependent redox reactions, where shifts in the redox peak potential (E_p) correlate to pH variations, often via a Nernstian relationship.[34] These sensors use proton-coupled electron-transfer (PCET) reactions involving redox-active materials whose equilibrium potential shifts with pH. A typical PCET reaction can be represented as

$$\mathrm{X} + \mathrm{e}^- + \mathrm{H}^+ \rightleftharpoons \mathrm{HX}$$

The equilibrium potential (E_eq) for this reaction, assuming unit activities for HX and X, ideally shifts by 59 mV per pH unit at 298 K:[35]

$$E_\mathrm{eq} = E^0 - \frac{RT}{F}\ln\left(\frac{a_\mathrm{HX}}{a_\mathrm{X} a_{\mathrm{H}^+}}\right)$$

$$= E^0 - \frac{RT}{F}\ln\left(\frac{a_\mathrm{HX}}{a_\mathrm{X}}\right) - \frac{\ln(10)\,RT}{F}\Delta\mathrm{pH} \approx E - 59\ \mathrm{mV}\ \Delta\mathrm{pH}\ (\mathrm{at\ T} = 298\ K)$$

In addition to rapid responsiveness, broad pH detection range, and durability, voltammetric pH sensors offer utility for electrolyzer research due to their compatibility with micro- and nanoprobe fabrication.[33] Traditional membrane-electrode assemblies (MEAs) used in electrolyzers consist of

membranes, catalyst layers, and gas-diffusion layers (GDLs), enclosed by flow fields, current collectors, and end plates. This assembly typically limits the use of conventional pH electrodes or optical sensors within the MEA structure. Conversely, it provides an opportunity for deploying voltammetric micro- and nanoelectrode sensors to measure local pH.

Here we use a nickel (Ni) mesh with a surface coating of $Ni(OH)_2/NiOOH$ redox couple as a local pH sensor within the BPM junction. We demonstrate that the Nernstian shift in the redox wave peak potential (E_{eq}) serves as an indicator of local pH conditions within the BPM junction, and particularly of pH changes under current flow. The ability to place the probe at different locations in the junction provides spatially resolved pH measurements, while rapid potential sweep rates afford temporal resolution.

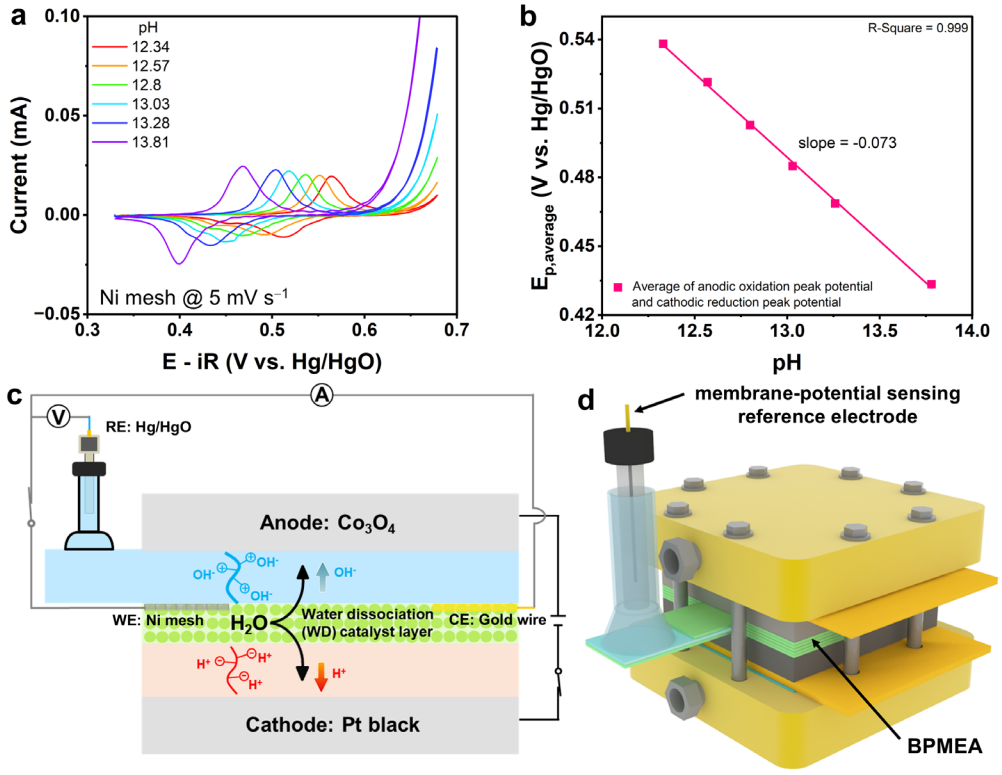

Figure 1. pH sensing with metal mesh electrodes. (a) Cyclic voltammograms of a Ni mesh pH sensor immersed in KOH electrolytes with known varied pH. All polarization curves were performed in Fe-free KOH at room temperature using a scan rate of 5 mV s^{-1}. Prior to measurement, Ni mesh was electrochemically reactivated by 500 CV cycles in 0.1 M Fe-free KOH to form a surface $Ni(OH)_2$ layer. (b) Average of anodic oxidation peak potential and cathodic reduction peak potential of the Ni

mesh probe vs. pH. (c) and (d) Bipolar membrane electrolyzer: pure water passes through the anode and cathode porous-transport layers (PTLs) and diffuses into the AEL and CEL junction where water is dissociated into H^+ and OH^- with the assistance of the WD catalyst in the electric field. A three-electrode system is introduced into the junction using the redox properties of Ni as the basis for pH sensing. The reference electrode here and in all experiments for this study was a Hg|HgO with 1.0 M NaOH filling solution that was calibrated by a HydroFlex hydrogen reference electrode (RHE).

Development of Ni-based local pH sensors for BPM. Our initial goal was to develop and demonstrate the use of a potentiometric pH probe that could be localized within the bipolar junction. Ni is well-suited as an electrode as it has a redox peak potential that is dependent on the electrolyte pH.[36, 37] Figure 1a shows the redox peak shifts to a more-negative potential as the pH increases. A linear fit indicates a slope of –73 mV per pH unit, slightly larger than the ideal Nernstian value of –59 mV per pH unit for a $1H^+/1e^-$ transfer. To further assess the fast time response, the Ni probe was subjected to cyclic voltammetry (CV) at a high scan rate of 2 V s^{-1}. Under these conditions, the average ($E_{\mathrm{p,average}}$) of anodic oxidation peak potential ($E_{\mathrm{p,a}}$) and cathodic reduction peak potential ($E_{\mathrm{p,c}}$) again exhibits a linear dependence on pH (Figure S1). Regardless of the details of the redox transformation, the pH dependence is useful for measuring pH at the Ni/NiO_x surface based on the oxidation peak potential.

A key challenge in building a voltammetric pH sensor for the BPM is the construction of a standalone three-electrode system inside the BPM electrolyzer to measure Ni redox. To minimize the effect of probe introduction on the thickness of the BPM junction, we used a commercial Ni grid and thinned it to ~1 μm by repeated electrochemical oxidation and acid etching (Figure S2). We then activated it to form a Ni (oxy)hydroxide surface layer by cyclic voltammetry (CV). A BPM electrolyzer fed by pure water was used as a platform to prevent other co-ions in the device from affecting the WD reaction, the transport of H^+ and OH^-, and the detection of pH. For the electrolyzer assembly (Figures 1c, 1d, and 2a), 0.2 wt% TiO_2 (commercial P25) was first spin-coated on the CEL as a WD catalyst layer, approximately 200 nm in thickness, where the catalyst loading or thickness has been optimized by our previous work.[10]

Subsequently, the activated Ni grid and Au fine wires were placed on the surface of the WD catalyst layer as the working electrode (WE) and counter electrode (CE), respectively. Another piece of AEL was laminated on the top. An AEL membrane-sensing strip was attached to the AEL of the

BPM and extended to the outside of the electrolyzer to connect a reference electrode.[17, 20] This configuration establishes an independent three-electrode system for measuring local pH changes within the BPM junction. Polarization curves of BPM electrolyzers are nearly identical in the presence and absence of the pH sensor (Figure S3).

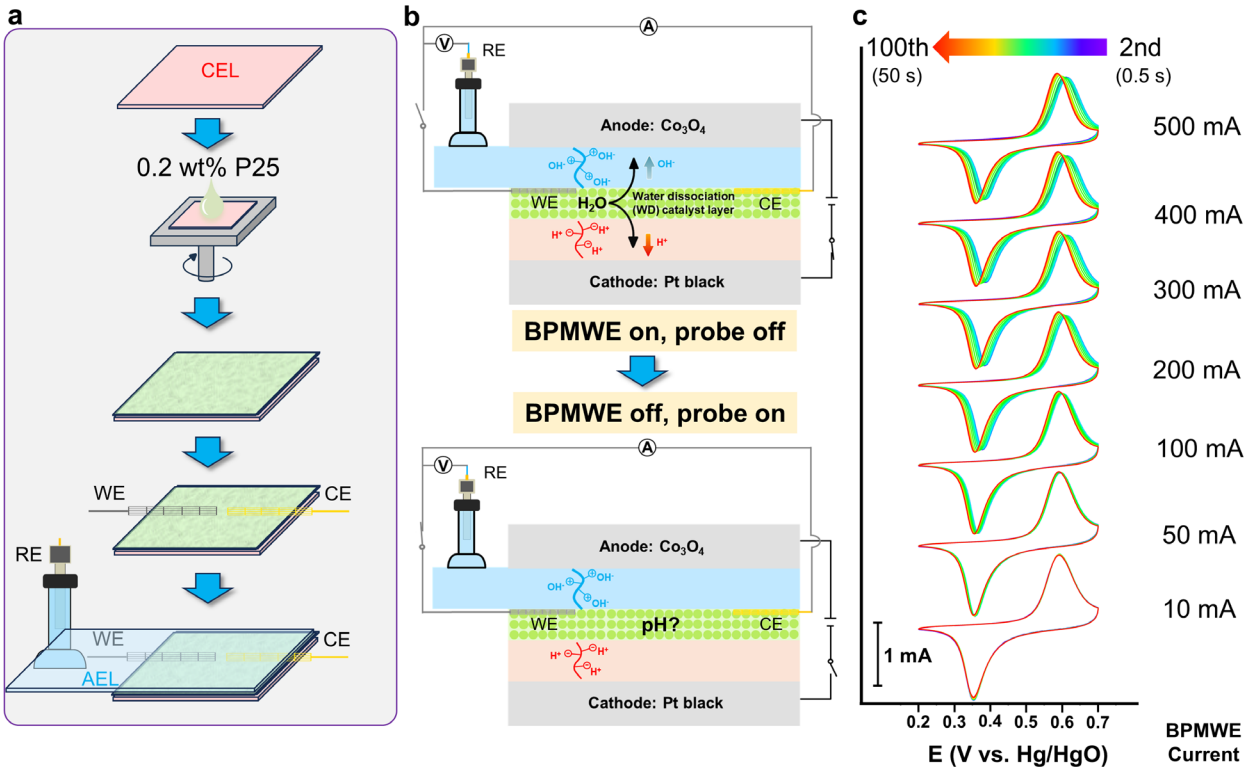

Figure 2. Integrating a pH probe in the BPM. (a) BPM assembly with WD catalyst and integrated three-electrode system for pH sensing. (b) Design showing the pH sensing system at open circuit while the BPM electrolyzer was subjected to different constant currents (10 mA to 500 mA). After a 2-min constant-current hold, electrolyzer was turned off and the pH sensing system was immediately started to perform the CV tests at a scan rate of 2.0 V s^{-1} within a potential window of 0.2–0.7 V vs. Hg/HgO. (c) Comparison of redox peak shifts for the Ni probe over 100 cycles after the BPM electrolyzer chronopotentiometry test.

Measurement and analysis of transient behavior after polarization. To determine how the pH in the junction varies under BPM operation, the electrolyzer (fed 18.2 MΩ·cm deionized water) is

first subjected to a constant current for 2 min, while the Ni pH sensor is at open circuit. Immediately after stopping the electrolysis current, a CV test was conducted at a scan rate of 2.0 V s^{-1} using the probe's three-electrode system (Figure 2b).

Making the pH measurement after, and not during, the application of electrolysis current is important. Under electrolysis, there is an additional electric potential drop through the bipolar membrane associated with driving the ion migration current at steady state. When the net electrolysis current is stopped, the electric potential associated with driving ion migration would be expected to discharge much faster than that associated with concentration polarization that results in a pH gradient (see section below on comparison to a non-PECT probe reaction).

In this case the Ni electrode is placed on the WD catalyst interface with the AEL, which is expected to be initially locally basic. Increasing the applied steady-state current density prior to the transient pH analysis resulted in an increased positive shift of $E_{p,a}$ and $E_{p,c}$, and thus a larger decrease in pH (Figure 2). This result is consistent with both the H^+ and OH^- being driven from the BPM junction region under reverse bias current resulting in a reduction of both ion concentrations, that is, resulting in a less basic local environment at the AEL, and likely less acidic at the CEL. We found that, following electrolyzer operation, the Ni redox features then shifted back negatively as a function of time (Figure 2, compare the CV cycle 2, purple, to CV cycle 100, red), showing the timescale for return from the steady-state local pH under current flow to that at the equilibrium condition.

In the time series of the post-electrolysis CVs in the junction, however, the Ni redox feature unexpectedly first shifts positively from the 2nd (purple) to the ~10th (blue) cycle (Figure. S4), indicating a shift to even lower pH after the electrolysis current was immediately stopped, prior to the return to the initial position. This feature is more pronounced in the BPM electrolyzer after running at higher current. One possibility may be a dissimilar rate constant for H^+ exchange between the water and the WD catalyst surface, and H^+ exchange between water molecules.[38, 39] This might be explained by the WD catalyst surface being able to exchange H^+ rapidly on short timescales, with the bulk ionization of H_2O is significantly slower ($k_{wd} \approx 10^{-5}$ s^{-1}) with therefore water molecules exchanging H^+ on longer timescales.[3, 40] The initial reduction of pH may be due to H^+ donation from the WD catalyst to the water, which transiently consumes local OH^- until a new equilibrium is established. In addition, the higher mobility of protons relative to hydroxide

ions may further contribute. Upon current interruption, OH^- and H^+ generation ceases and the residual electric field must discharge, producing a migration current through the entire cell. During this ions' redistribution, protons driven previously in the same direction of the applied current may move back more rapidly than hydroxides, giving rise to the observed transient pH shift.

Afterwards, the CV curves for all tests gradually returned to an $E_{\mathrm{p,average}}$ at ~0.47 V vs. Hg/HgO (this would be associated with the equilibrium pH of 13.4 in that region of the BPM, assuming no systemic offsets of the Ni sensor). These observations show the pH probe can measure steady-state pH polarization that occurs as a function of operating current through the BPM junction.

We next performed 300 CV cycles on the Ni probe continuously at 2.0 V s^{-1} within a potential window of 0.2–0.75 V vs. Hg/HgO while the BPM electrolyzer was periodically switched between open-circuit potential (OCP) and chronopotentiometry, each process lasting 33 s, which corresponds exactly to the completion of 60 CV cycles for pH sensing. In Figure 3a, a Ni pH probe was placed on a WD catalyst layer prepared by spin-coating with 0.2 wt% P25 ink on the CEL. Subsequently, a piece of AEL was covered on top of the probe and the catalyst layer. All the $E_{\mathrm{p,average}}$ of Ni probe were extracted from CV curves as a function of cycle number and BPM electrolyzer on and off states.

The CV curves of the Ni probe quickly reach a steady state during the first 60 cycles, when no current passes through the BPM (Figure S5). However, upon application of a constant electrolysis current, the probe oxidation peak immediately shifted positively and stabilized within ~5 s. This indicates that when the electrolyzer was switched on, the OH^- concentration at the interface of the TiO_2 catalyst and the AEL dropped dramatically, resulting in an apparent decrease in pH. In addition to changes in local pH, the peak is shifted by electrostatic potential drops through the membrane associated with driving the migration curve that are difficult to deconvolute under current flow conditions.

The cell was subsequently returned to open circuit and the temporal changes in CV response and local pH followed the trend discussed previously in Figure 2c. To rule out the changes in the voltammogram due to ohmic drops specifically through the AEL due to the electrolysis current flowing from anode to cathode, we calculated the approximate ohmic drop through the membrane during operation (Figure S6). We used PiperION-A40-HCO_3 (TP-85, 40-μm thick, Versogen)

membrane as AEL and a membrane-potential-sensing strip. TP-85 ionic conductivity is ~80 mS cm^{-1} at 25 °C.[41] Taking 100 mS cm^{-1} at 55 °C the areal ionic resistance of the AEL is ~0.04 Ω cm^{-1}. This corresponds to an ohmic drop of 8 mV at 200 mA cm^{-2} cell current, a small value relative to the $E_{\mathrm{p,average}}$ shift of ~90 mV. Note that this small ohmic drop within the membrane does not mean that under current flow there is no significant ohmic drop elsewhere. An ohmic drop is expected to also develop within the WD catalyst layer where the ion concentrations are lower.

We subsequently altered the distance of the Ni probe from the AEL to study the spatial pH profile in the WD catalyst layer. We used the same coating method as before, with 0.2 wt% P25 ink spun onto the CEL to minimize artifacts and the influence from the CEL interface. Here catalyst layers with different thicknesses were also spin-coated on the AEL using 0.1, 0.2, and 0.5 wt% P25 inks, prior to sandwiching the Ni mesh in-between the two catalyst layers. Based on previous calibration,[10] these ink concentrations yield WD catalyst-layer thicknesses of approximately 100, 200, and 520 nm, respectively. We again found that the shift of the redox peak was proportional to the applied current indicating that with current through the cell increases so does the pH polarization within the BPM junction. For instance, the $E_{\mathrm{p,average}}$ of Ni probe shifted by ~90 mV at a current of 200 mA cm^{-2} applied over the electrolyzer, compared to only ~20 mV at 25 mA cm^{-2}, corresponding to decreases of approximately 1.36 and 0.30 pH units, respectively. However, as the distance between the probe and the AEL increased, the positive shift of the $Ni(OH)_2$ oxidation peak became smaller when the same current was passed through the BPM. This result indicates that after the BPM electrolyzer turns on, the pH at the AEL interface within the junction decreases significantly, while the pH changes are less pronounced in regions farther from the AEL. Assuming the AEL is completely in the OH^- form and the CEL in the H^+ form, the pH decreases from ~14 to ~0 from the AEL interface to the CEL interface,[10] but the alkalinity of the region close to the AEL decreases as reverse bias is applied, indicating that the pH gradient within the BPM junction diminishes.

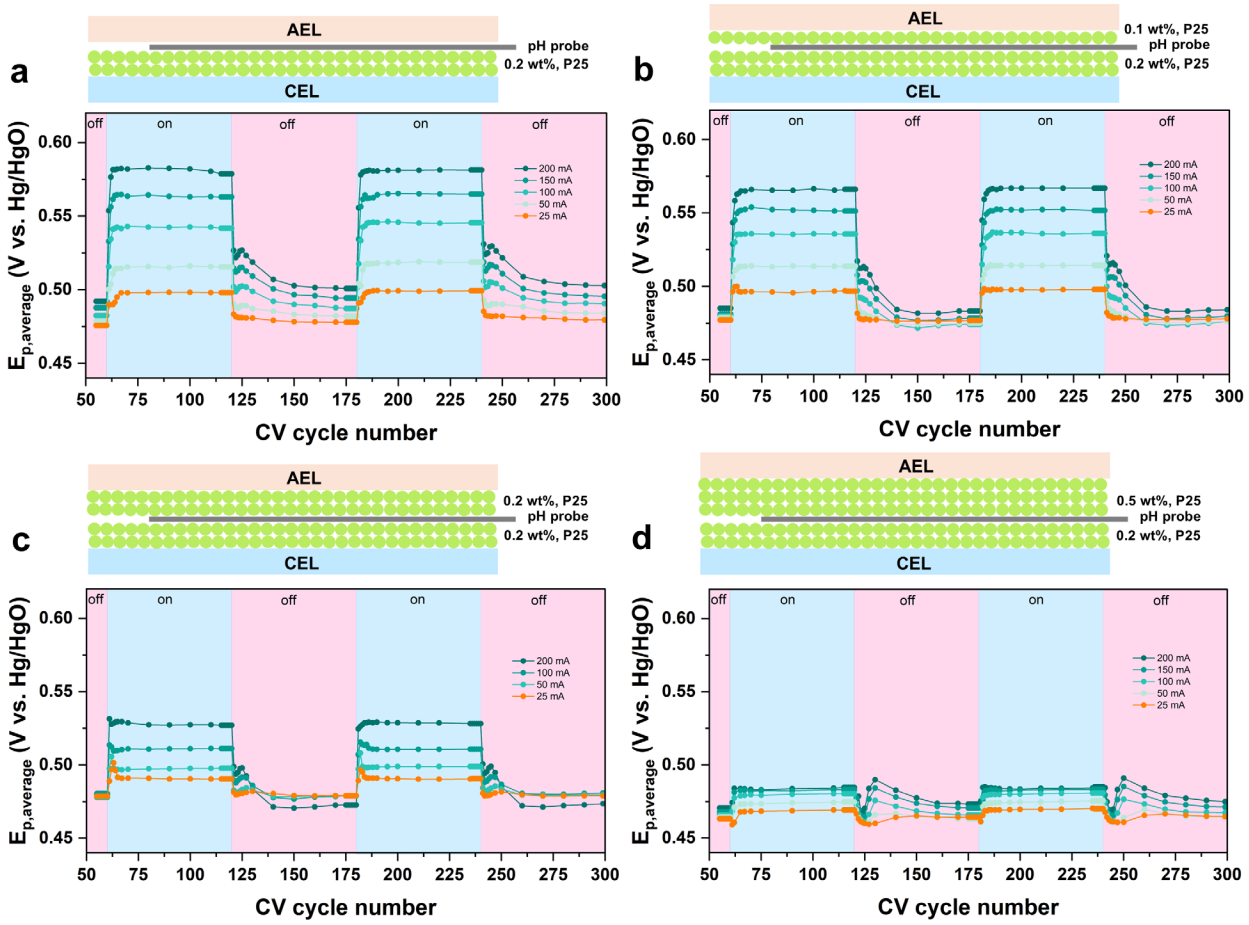

Figure 3. Current through the BPM junction causes spatially dependent pH polarization. (a) Redox peak potential ($E_{\mathrm{p,average}}$) response of the Ni probe as a function of the CV cycle number when periodic OCV (off) and chronopotentiometry (on) applied to the BPM electrolyzer under reverse-bias conditions. In this case, the CEL was coated with 0.2 wt% TiO_2 ink and the probe was attached directly to the AEL. (b) Redox peak potential ($E_{\mathrm{p,average}}$) response of the Ni probe upon introducing a WD catalyst layer between the AEL and pH probe by spin-coating 0.1 wt% TiO_2 ink on the AEL while maintaining a constant catalyst thickness on the CEL. (c) Investigation of the redox peak potential ($E_{\mathrm{p,average}}$) response of the Ni probe achieved by spin-coating 0.2 wt% TiO_2 ink on the AEL and CEL, respectively. (d) Further increase the catalyst thickness on the AEL by spin-coating 0.5 wt% TiO_2 ink on AEL for the study of redox peak potential ($E_{\mathrm{p,average}}$) response of the Ni probe. We note that we cannot rule out a systematic offset from unaccounted-for interface potentials when quantifying the exact pH value by our calibration cure, the PZC of TiO_2 can be obtained through titration. TiO_2 acts as a buffer, and the pH in the middle of the junction will equal the PZC value of TiO_2 (~ 6). This is a way to estimate what the absolute pH are most likely to be.

The $E_{p,a}$ shifts under reverse and forward biases. In the BPM junction, WD under reverse bias ($H_2O \rightarrow H^+ + OH^-$) and H^+/OH^- recombination under forward bias are two opposite processes.[42] In forward bias the expected opposite shift of the Ni probe oxidation peak was observed (Figure 4a). The shift at –50 mA cm^{-2} in forward bias (with the cathode-anode connections of the electrolyzer unchanged) is roughly -15 mV, and similar to the shift in reverse bias at the 50 mA cm^{-2} of about +10 mV. In forward-bias operation H^+ and OH^- ions migrate into the junction, where they recombine to form water. Due to the migration of OH^- from the AEL, the local pH increases, corresponding to the negative shifts of the probe oxidation peak.

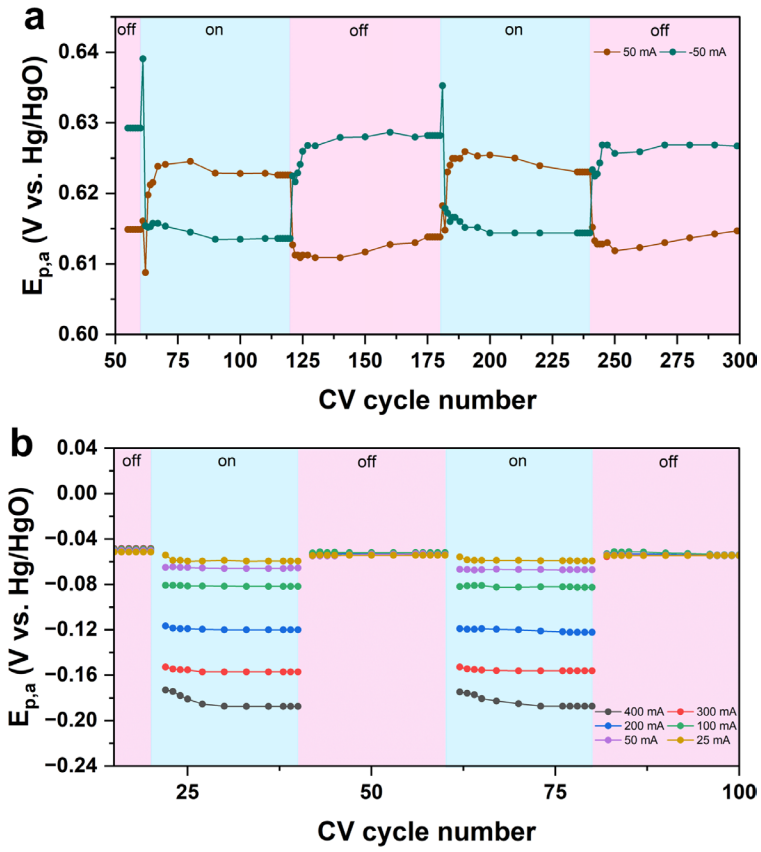

Figure 4. Forward and reverse current and comparison to a non-PCET probe reaction. (a) Oxidation peak potential response of the Ni probe as a function of CV cycle number during periodic OCV (off) and chronopotentiometry (on) applied to the BPM electrolyzer. The BPM was operated under forward and reverse bias conditions, with applied currents of +50 mA and –50 mA, respectively. Following the +50 mA operation, the cell was run at –50 mA cm^{-2} for 20 min prior to conducting the pH sensing experiment at –50 mA. The observed shifts in oxidation peak potential reflect dynamic changes in local pH within the BPM

junction under varying bias directions. (b) Oxidation peak potential response of the poly(vinylferrocene)/carbon fiber during periodic on/off operation of the BPM electrolyzer. The CV tests were performed at a scan rate of 1.0 V s^{-1} within a potential window of 0.10 to –0.50 V vs. Hg/HgO. Note the $E_{p,a}$ shifts for the ferrocene group return immediately to the original position when the electrolysis current is turned off, consistent with the non-PCET process being insensitive to the local pH.

Comparison to non-PECT probe reaction. To distinguish the effect of the electric potential drop within the BPM junction in comparison to pH concentration polarization, poly(vinylferrocene) was employed as a non-pH-responsive electrochemical probe. Initially, poly(vinylferrocene) was electrodeposited onto carbon fibers and characterized in 0.10 M KCl solution, displaying a distinctive redox peak in the CV curve (Figure S8). Subsequently, the poly(vinylferrocene)-modified carbon fiber probe was introduced into the BPM junction, where 0.2 wt% and 0.5 wt% P25 inks had been spin-coated onto the CEL and AEL, respectively. Under an applied reverse bias across the BPM, the oxidation peak potential of poly(vinylferrocene) exhibited a negative shift (Figure 4b).

The observed negative shift of the poly(vinylferrocene) oxidation peak under bias likely reflects a convolution of migration-related ohmic losses in the depleted AEL interfacial region and dynamic changes in Donnan potentials at the membrane/solution interfaces, both of which modify the local electrostatic potential experienced by the redox probe relative to the reference electrode electrostatic potential. Although poly(vinylferrocene) exhibits peak potential shifts with increasing current, no transient behavior is observed during on–off cycling. That is, the peak potential shifts back to its initial potential immediately on the timescale of the CV measurements, consistent with the ferrocene redox processes unaffected by the local pH changes. This behavior is distinct from the proton-coupled electron transfer processes measured on the Ni probe (nominally $NiOOH + e^- + H_2O \rightleftarrows Ni(OH)_2 + OH^-$). We therefore use this data to conclude that the primary potential shift for the Ni electrode measured on the timescale of the CV response is pH polarization, or equivalently, ion concentration relaxation, rather than electrostatic effects, given the fast time scale for relaxation of the other electrostatic effects after the electrolysis current is stopped.

The physical picture of local pH and acid-base chemistry in the BPM junction. The PZC is a key property of metal oxides, indicating the pH at which the surface of the oxide has a zero net

surface charge.[43] This occurs when the number of positive and negative surface charges is equal, and thus the surface exhibits no electrostatic attraction or repulsion for surrounding ions. The PZC is a materials-specific parameter that describes the interaction of the metal-oxide surface with ions, adsorbates, and solvents.[44] When the pH < PZC, the surface of the catalyst is positively charged due to the adsorption of protons.[38] This positive charge, in turn, induces the oxygen atoms of water molecules to, an average, orient toward the catalyst surface.[45] When the pH >PZC, the surface is negatively charged and the hydrogen atoms from water molecules, on average, orient toward the catalyst surface. With respect to the TiO_2 catalyst (PZC ~5.8-6.8 for anatase), we expect different interfacial charging properties within the BPM junction due to the presence of the pH gradient.[3, 38] Near the AEL, the TiO_2 surface is expected to take on a negative charge due to deprotonation (pH > PZC), which affects the orientation of water molecules at the catalyst surface. The extent of surface deprotonation (surface negative charge density) should decrease as the pH is more acidic further from the AEL (Figure 5a). Near the CEL, the TiO_2 surface becomes protonated as pH < PZC. This would yield a corresponding positive charge distribution within the catalyst layer, driven by the local acidic environment.

From the perspective of the entire BPM junction, the surface-charge density on the TiO_2 WD catalyst likely varies across the junction with the gradient in pH. The interaction between water molecules and interfacial charges influences the orientation or disorder (entropy) of interfacial water molecules,[26, 45] which is likely connected to the proton-transport rate in the aqueous phase.

The pH probe results in Figure 2c and Figure 3 indicate that when a reverse-bias current is applied, the local pH near the AEL decreases, corresponding to a reduced degree of deprotonation on the catalyst surface. For this system, we thus propose a catalyst-mediated proton-transfer mechanism, as shown in Figure 5b and 5c. Under the influence of the electric field, OH^- ions in the AEL migrate toward the anode of the MEA, driving the free OH^- ions at the AEL interface into the membrane to maintain charge balance between the fixed positive charges and the free anions within the membrane.[20] The migration of OH^- at the membrane interface results in a local pH decrease, whereby negatively charged Ti-O^- site tends to capture a proton from water facilitated by hydrogen bonding, leading to WD and the generation of OH^- ions. Protons may then transport across the titania surface or through surface water networks, for example, adjacent Ti-O^- site protonates, generating OH^- ions, which may deprotonate other surface sites. In this process, hydrogen bond

networks could aid in the mobility of hydroxide ions across the surface bridging nearby Ti-OH or Ti-O^- sites.[46]

As the driving force for WD, and hence the local electric fields increase, OH^- are driven from the catalyst region into the AEL and toward the anode. The WD reaction occurring on the surfaces of the TiO_2 regenerate OH^- to replace those transported out, however, because free energy is consumed during the process, as quantified by η_{wd}, the steady state OH^- and H^+ concentrations in the WD catalyst region necessarily decreases from their equilibrium values. This explains the apparent decrease in pH at the AEL interface, where OH^- is the dominant carrier, and the expected increase in pH at the CEL, where H^+ is the dominant carrier.

The proposed increase pH near the CEL under reverse bias current flow would cause the protonated catalyst surface to release H^+ ions, while hydronium (H_3O^+) ions in water re-establish a new protonated surface with the Ti-OH group through hydrogen bonding. Subsequently, the adjacent Ti-OH_2^+ site completes the cycle of proton release and re-acquisition. This pathway may allow for fast proton hopping along the surface without requiring the movement of H^+ through a series of protonation and deprotonation steps on different water molecules. The formation and breaking of hydrogen bonds throughout the process is pivotal for the transfer of protons from one Ti-OH group to another.[47]

Overall, in the BPM junction, the protonated or deprotonated surfaces of TiO_2, influenced by the changes in pH gradient, may serve as sites for the release or capture of protons, mediating the rapid transport of OH^- and H^+ ions resulting from WD.

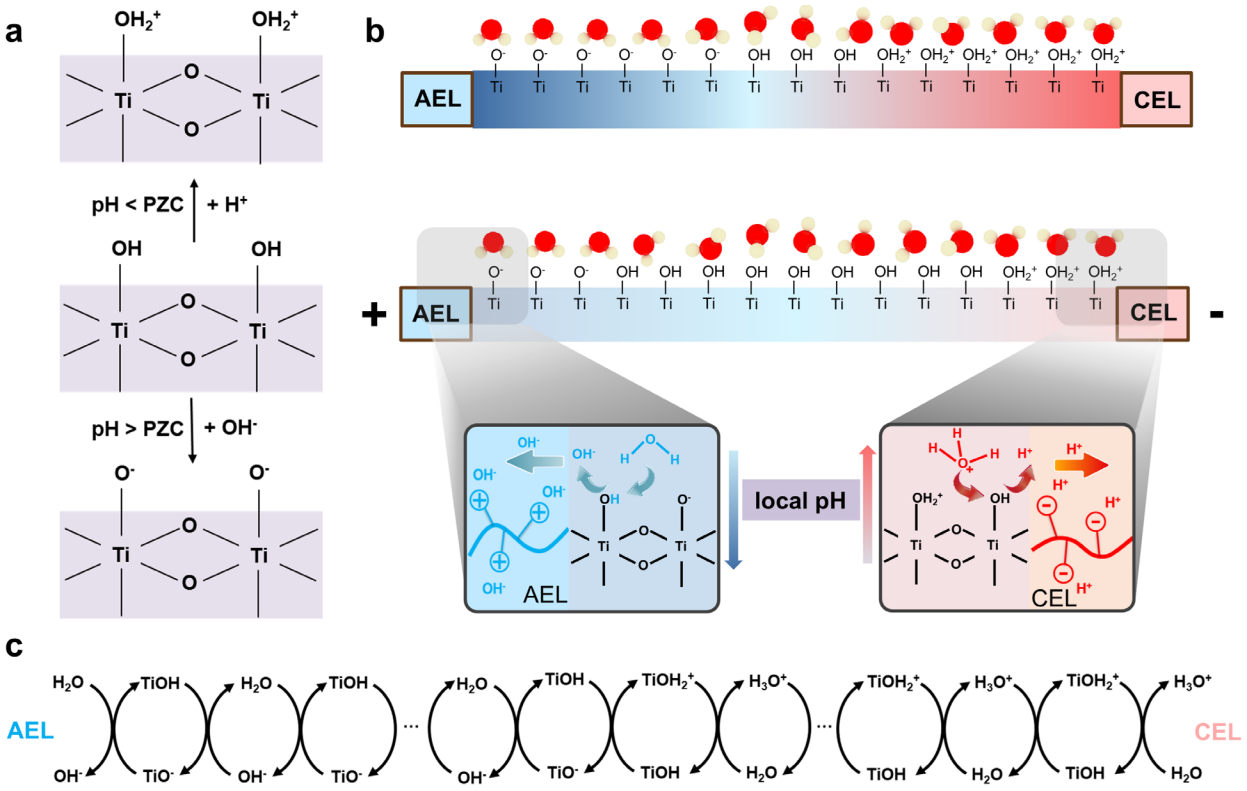

Figure 5. Possible physical picture of local pH and WD. (a) The correlation between PZC and the surface charge characteristics of TiO_2. (b) Possible interfacial structures of WD catalysts in BPM under static and biased conditions, respectively, including the schematic orientation of water molecules and surface-charge characteristics of catalysts. The magnified illustrations depict the possible OH^- migration mechanism on the AEL side and the H^+ transport mechanism on the CEL side, respectively. (c) Simplified mechanism for voltage-driven WD on TiO_2. Under reverse bias, the deprotonated catalyst surface at the AEL interfacial region facilitates WD and OH^- migration, while the protonated TiO_2 surface at the CEL interface accelerates H^+ hopping.

In summary, we developed a Ni based pH probe in BPM electrolyzers by integrating it with the membrane-potential-sensing method. By leveraging the pH dependence of the redox-peak potential of (oxy)hydroxides on Ni, an ultrathin Ni mesh was placed at different positions within the WD catalyst layer of the BPM, revealing pH variations under on/off states of the electrolyzer and further informing on the voltage-driven WD mechanism. After the removal of reverse bias electrolyzer current, the redox peak of the probe exhibited a slight positive shift followed by a significant negative shift in potential, which became more pronounced as the current applied to the

BPM electrolyzer increased. This result indicates that the local pH near the AEL initially decreases, then increases, as it relaxes to the equilibrium distribution of ions.

The applied currents and electric-field redistribution lead to a reduction in OH^- concentration within the AEL-side of the BPM junction, as indicated by the positive shift of the redox peak. However, the magnitude of this change is closely related to the position of the probe within the catalyst layer; the decrease in pH is most pronounced at the AEL interface, while the localized pH changes diminish with increasing distance from the AEL. This result indicates that, after the operation of the BPM electrolyzer, the pH gradient within its junction is reduced. Consequently, we propose a possible mechanism for the transfer of H^+ and OH^- facilitated by the surface protonated and deprotonated TiO_2 catalysts. Influenced by the pH gradient within BPM, the protonated or deprotonated surfaces of TiO_2 may serve as sites for proton release or reception, mediating the migration of OH^- ions and H^+ hopping in the presence of electric fields.

The new experimental strategy demonstrated in this work both aids in understanding the WD mechanism in BPM and can also be applied to a wider range of catalytic interfaces and processes occurring in other electrolyzer-type structures. Specifically, when a reverse bias is applied to the BPM, the pH gradient across the junction appears reduced. Under these conditions, several factors are likely important in determining the WD rate, including the charge state of the WD catalyst surface, the strength of water-catalyst interactions, changes in the hydrogen-bond network, and the entropy of the interfacial water layer. Because all these factors likely depend on local pH, the results of this study imply WD catalysts might be improved by accounting for dynamic changes in local pH with current across the junction, for example by tuning surface-charge or surface-acidity gradients. By coupling pH-dependent redox transformations on electrode probes with pH-independent redox transformations, information regarding pH and potential distributions in operating electrochemical cells can be collected.

The limitation of this study lies in the lack of further evidence supporting the proposed mechanism, the lack of absolute calibration of the Ni sensor in the junction, and the instability of the sensor in the acidic CEL side of the BPM junction. The complexity of the BPM junction and its buried interface will continue to present challenges and opportunities for investigation. Developing thinner probes and materials with a broader range and higher sensitivity for pH measurement will

be significant for elucidating the pH and electric-potential profile within the WD catalyst layer, as well as coupling them to spectroscopic techniques.

ASSOCIATED CONTENT

Supporting Information

The Supporting Information is available free of charge at http://pubs.acs.org.

Materials fabrication, characterization, membrane potential sensing construction, electrolyzer assembly, and electrochemical measurements.

AUTHOR INFORMATION

Corresponding Author

Shannon W. Boettcher – *Department of Chemical & Biomolecular Engineering and Department of Chemistry, University of California, Berkeley, and Energy Storage and Distributed Resources Division, Lawrence Berkeley National Laboratory, Berkeley, CA 94720, USA; Oregon Center for Electrochemistry, Department of Chemistry and Biochemistry, University of Oregon, Eugene, OR 97403, USA;* orcid.org/0000-0001-8971-9123.

Email: boettcher@berkeley.edu

Authors

Shujin Hou – *Department of Chemical & Biomolecular Engineering and Department of Chemistry, University of California, Berkeley, and Energy Storage and Distributed Resources Division, Lawrence Berkeley National Laboratory, Berkeley, CA 94720, USA; Oregon Center for Electrochemistry, Department of Chemistry and Biochemistry, University of Oregon, Eugene, OR 97403, USA;* orcid.org/0000-0002-3633-2387.

Email: shujinhou@berkeley.edu

T. Nathan Stovall – *Department of Chemical & Biomolecular Engineering and Department of Chemistry, University of California, Berkeley, and Energy Storage and Distributed Resources Division, Lawrence Berkeley National Laboratory, Berkeley, CA 94720, USA.*

Email: nstovall@berkeley.edu

Adam Z. Weber – *Energy Storage and Distributed Resources Division, Lawrence Berkeley National Laboratory, Berkeley, CA 94720, USA.*

Email: AZWeber@lbl.gov

Author contributions

S.H. and S.W.B. conceptualized and led the project. S. H. and T.N.S. conducted experiments, collected electrolyzer data, and characterized samples. T.N.S. and A.Z.W. provided feedback on the experiments and data analysis. S.H., T.N.S., and S.W.B. wrote the original draft and all authors reviewed and edited the manuscript.

Notes

The authors declare there are no other conflicts of interest.

ACKNOWLEDGMENTS

This work was supported by the U.S. Department of Energy (DOE), Office of Science Energy Earthshot Initiative as part of the Center for Ion Management in Electrochemical Systems (CIMES), award DE-SC0024713. Partial support measuring local pH was funded by the U.S. Office of Naval Research, award N00014-25-1-2256. This work utilized shared instrumentation at the Center for Advanced Materials Characterization in Oregon (CAMCOR) and the Phil and Penny Knight Campus for Accelerating Scientific Impact. Lihaokun Chen and Paul Kempler are acknowledged for assistance and insightful discussions on this project.

REFERENCES

(1) Li, A.; Kong, S.; Adachi, K.; Ooka, H.; Fushimi, K.; Jiang, Q.; Ofuchi, H.; Hamamoto, S.; Oura, M.; Higashi, K.; et al. Atomically dispersed hexavalent iridium oxide from MnO_2 reduction for oxygen evolution catalysis. *Science* **2024**, *384* (6696), 666-670. DOI: 10.1126/science.adg5193.

(2) Klingenhof, M.; Trzesniowski, H.; Koch, S.; Zhu, J.; Zeng, Z.; Metzler, L.; Klinger, A.; Elshamy, M.; Lehmann, F.; Buchheister, P. W.; et al. High-performance anion-exchange membrane water electrolysers using NiX (X = Fe,Co,Mn) catalyst-coated membranes with redox-active Ni–O ligands. *Nat. Catal.* **2024**, *7* (11), 1213-1222. DOI: 10.1038/s41929-024-01238-w.

(3) Oener, S. Z.; Foster, M. J.; Boettcher, S. W. Accelerating water dissociation in bipolar membranes and for electrocatalysis. *Science* **2020**, *369* (6507), 1099-1103. DOI: 10.1126/science.aaz1487.

(4) Li, S.; Zhou, Y.; Fu, X.; Pedersen, J. B.; Saccoccio, M.; Andersen, S. Z.; Enemark-Rasmussen, K.; Kempen, P. J.; Damsgaard, C. D.; Xu, A.; et al. Long-term continuous ammonia electrosynthesis. *Nature* **2024**, *629* (8010), 92-97. DOI: 10.1038/s41586-024-07276-5.

(5) Birdja, Y. Y.; Pérez-Gallent, E.; Figueiredo, M. C.; Göttle, A. J.; Calle-Vallejo, F.; Koper, M. T. M. Advances and challenges in understanding the electrocatalytic conversion of carbon dioxide to fuels. *Nat. Energy* **2019**, *4* (9), 732-745. DOI: 10.1038/s41560-019-0450-y.
(6) Fu, X.; Xu, A.; Pedersen, J. B.; Li, S.; Sazinas, R.; Zhou, Y.; Andersen, S. Z.; Saccoccio, M.; Deissler, N. H.; Mygind, J. B. V.; et al. Phenol as proton shuttle and buffer for lithium-mediated ammonia electrosynthesis. *Nat. Commun.* **2024**, *15* (1), 2417. DOI: 10.1038/s41467-024-46803-w.
(7) van der Ham, C. J.; Koper, M. T.; Hetterscheid, D. G. Challenges in reduction of dinitrogen by proton and electron transfer. *Chem. Soc. Rev.* **2014**, *43* (15), 5183-5191. DOI: 10.1039/c4cs00085d.
(8) Blommaert, M. A.; Aili, D.; Tufa, R. A.; Li, Q.; Smith, W. A.; Vermaas, D. A. Insights and Challenges for Applying Bipolar Membranes in Advanced Electrochemical Energy Systems. *ACS Energy Lett.* **2021**, *6* (7), 2539-2548. DOI: 10.1021/acsenergylett.1c00618.
(9) Bui, J. C.; Lees, E. W.; Liu, A. K.; Toh, W. L.; Stovall, T. N.; Goyal, P.; Galang, F. J. U.; Surendranath, Y.; Bell, A. T.; Weber, A. Z. Ion-specific phenomena limit energy recovery in forward-biased bipolar membranes. *Nat. Chem. Eng.* **2024**, *2* (1), 63-76. DOI: 10.1038/s44286-024-00154-x.
(10) Chen, L.; Xu, Q.; Oener, S. Z.; Fabrizio, K.; Boettcher, S. W. Design principles for water dissociation catalysts in high-performance bipolar membranes. *Nat. Commun.* **2022**, *13* (1), 3846. DOI: 10.1038/s41467-022-31429-7.
(11) Lucas, É.; Bui, J. C.; Stovall, T. N.; Hwang, M.; Wang, K.; Dunn, E. R.; Spickermann, E.; Shiau, L.; Kusoglu, A.; Weber, A. Z.; et al. Asymmetric Bipolar Membrane for High Current Density Electrodialysis Operation with Exceptional Stability. *ACS Energy Lett.* **2024**, *9* (11), 5596-5605. DOI: 10.1021/acsenergylett.4c01662.
(12) Vulpin, O. T.; Mitchell, J. B.; Chen, L.; Lim, J.; Sasmal, S.; Price, N. G.; Jarvis, S. R.; Boettcher, S. W. Comparing Advanced Bipolar Membranes for High-Current Electrodialysis and Membrane Electrolysis. *ACS Energy Lett.* **2025**, *10* (2), 845-852. DOI: 10.1021/acsenergylett.4c03538.
(13) Unlu, M.; Zhou, J.; Kohl, P. A. Hybrid polymer electrolyte fuel cells: alkaline electrodes with proton conducting membrane. *Angew. Chem. Int. Ed.* **2010**, *49* (7), 1299-1301. DOI: 10.1002/anie.200906021.

(14) Petrov, K. V.; Koopman, C. I.; Subramanian, S.; Koper, M. T. M.; Burdyny, T.; Vermaas, D. A. Bipolar membranes for intrinsically stable and scalable CO_2 electrolysis. *Nat. Energy* **2024**, *9* (8), 932-938. DOI: 10.1038/s41560-024-01574-y.

(15) Yu, W.; Zhang, Z.; Luo, F.; Li, X.; Duan, F.; Xu, Y.; Liu, Z.; Liang, X.; Wang, Y.; Wu, L.; et al. Tailoring high-performance bipolar membrane for durable pure water electrolysis. *Nat. Commun.* **2024**, *15* (1), 10220. DOI: 10.1038/s41467-024-54514-5.

(16) Luo, F.; Yu, W.; Li, X.; Liang, X.; Li, W.; Duan, F.; Wang, Y.; Ge, X.; Wu, L.; Xu, T. Enhanced bipolar membranes for durable ampere-level water electrolysis. *Energy Environ. Sci.* **2025**, *18* (2), 728-737. DOI: 10.1039/d4ee04524f.

(17) Sasmal, S.; Chen, L.; Sarma, P. V.; Vulpin, O. T.; Simons, C. R.; Wells, K. M.; Spontak, R. J.; Boettcher, S. W. Materials descriptors for advanced water dissociation catalysts in bipolar membranes. *Nat. Mater.* **2024**, *23* (10), 1421-1427. DOI: 10.1038/s41563-024-01943-8.

(18) Gao, T.; Schulte, L.; Xiao, L.; Yamamoto, E.; Metlay, A. S.; Sheehan, C. J.; Marth, S.; Park, H.; Sasmal, S.; Galang, F. J.; et al. Bipolar Membranes With Controlled, Microscale 3D Junctions Enhance the Rates of Water Dissociation and Formation. *Adv. Energy Mater.* **2025**, *15*, 2404285. DOI: 10.1002/aenm.202404285.

(19) Yan, Z.; Zhu, L.; Li, Y. C.; Wycisk, R. J.; Pintauro, P. N.; Hickner, M. A.; Mallouk, T. E. The balance of electric field and interfacial catalysis in promoting water dissociation in bipolar membranes. *Energy Environ. Sci.* **2018**, *11* (8), 2235-2245. DOI: 10.1039/c8ee01192c.

(20) Chen, L.; Xu, Q.; Boettcher, S. W. Kinetics and mechanism of heterogeneous voltage-driven water-dissociation catalysis. *Joule* **2023**, *7* (8), 1867-1886. DOI: 10.1016/j.joule.2023.06.011.

(21) Delley, M. F.; Nichols, E. M.; Mayer, J. M. Interfacial Acid-Base Equilibria and Electric Fields Concurrently Probed by In Situ Surface-Enhanced Infrared Spectroscopy. *J. Am. Chem. Soc.* **2021**, *143* (28), 10778-10792. DOI: 10.1021/jacs.1c05419.

(22) Gonella, G.; Backus, E. H. G.; Nagata, Y.; Bonthuis, D. J.; Loche, P.; Schlaich, A.; Netz, R. R.; Kuhnle, A.; McCrum, I. T.; Koper, M. T. M.; et al. Water at charged interfaces. *Nat. Rev. Chem.* **2021**, *5* (7), 466-485. DOI: 10.1038/s41570-021-00293-2.

(23) Jungwirth, P. Spiers Memorial Lecture. Ions at aqueous interfaces. *Faraday Discuss.* **2009**, *141*, 9-30; discussion 81-98. DOI: 10.1039/b816684f.

(24) Hou, S.; Xu, L.; Ding, X.; Kluge, R. M.; Sarpey, T. K.; Haid, R. W.; Garlyyev, B.; Mukherjee, S.; Warnan, J.; Koch, M.; et al. Dual In Situ Laser Techniques Underpin the Role of Cations in

Impacting Electrocatalysts. *Angew. Chem. Int. Ed.* **2022**, *61* (24), e202201610. DOI: 10.1002/anie.202201610.

(25) Sarabia, F.; Gomez Rodellar, C.; Roldan Cuenya, B.; Oener, S. Z. Exploring dynamic solvation kinetics at electrocatalyst surfaces. *Nat. Commun.* **2024**, *15* (1), 8204. DOI: 10.1038/s41467-024-52499-9.

(26) Rodellar, C. G.; Gisbert-Gonzalez, J. M.; Sarabia, F.; Roldan Cuenya, B.; Oener, S. Z. Ion solvation kinetics in bipolar membranes and at electrolyte–metal interfaces. *Nat. Energy* **2024**, *9* (5), 548-558. DOI: 10.1038/s41560-024-01484-z.

(27) Bourikas, K.; Kordulis, C.; Lycourghiotis, A. Titanium dioxide (anatase and rutile): surface chemistry, liquid-solid interface chemistry, and scientific synthesis of supported catalysts. *Chem. Rev.* **2014**, *114* (19), 9754-9823. DOI: 10.1021/cr300230q.

(28) Ghoneim, M. T.; Nguyen, A.; Dereje, N.; Huang, J.; Moore, G. C.; Murzynowski, P. J.; Dagdeviren, C. Recent Progress in Electrochemical pH-Sensing Materials and Configurations for Biomedical Applications. *Chem. Rev.* **2019**, *119* (8), 5248-5297. DOI: 10.1021/acs.chemrev.8b00655.

(29) Lu, X.; Zhu, C.; Wu, Z.; Xuan, J.; Francisco, J. S.; Wang, H. In Situ Observation of the pH Gradient near the Gas Diffusion Electrode of CO_2 Reduction in Alkaline Electrolyte. *J. Am. Chem. Soc.* **2020**, *142* (36), 15438-15444. DOI: 10.1021/jacs.0c06779.

(30) Welch, A. J.; Fenwick, A. Q.; Böhme, A.; Chen, H.-Y.; Sullivan, I.; Li, X.; DuChene, J. S.; Xiang, C.; Atwater, H. A. Operando Local pH Measurement within Gas Diffusion Electrodes Performing Electrochemical Carbon Dioxide Reduction. *J. Phys. Chem. C* **2021**, *125* (38), 20896-20904. DOI: 10.1021/acs.jpcc.1c06265.

(31) Böhme, A.; Bui, J. C.; Fenwick, A. Q.; Bhide, R.; Feltenberger, C. N.; Welch, A. J.; King, A. J.; Bell, A. T.; Weber, A. Z.; Ardo, S.; et al. Direct observation of the local microenvironment in inhomogeneous CO_2 reduction gas diffusion electrodes via versatile pOH imaging. *Energy Environ. Sci.* **2023**, *16* (4), 1783-1795. DOI: 10.1039/d2ee02607d.

(32) Munteanu, R. E.; Stanica, L.; Gheorghiu, M.; Gaspar, S. Measurement of the Extracellular pH of Adherently Growing Mammalian Cells with High Spatial Resolution Using a Voltammetric pH Microsensor. *Anal. Chem.* **2018**, *90* (11), 6899-6905. DOI: 10.1021/acs.analchem.8b01124.

(33) Monteiro, M. C. O.; Jacobse, L.; Touzalin, T.; Koper, M. T. M. Mediator-Free SECM for Probing the Diffusion Layer pH with Functionalized Gold Ultramicroelectrodes. *Anal. Chem.* **2020**, *92* (2), 2237-2243. DOI: 10.1021/acs.analchem.9b04952.

(34) Michalak, M.; Kurel, M.; Jedraszko, J.; Toczydlowska, D.; Wittstock, G.; Opallo, M.; Nogala, W. Voltammetric pH Nanosensor. *Anal. Chem.* **2015**, *87* (23), 11641-11645. DOI: 10.1021/acs.analchem.5b03482.

(35) Walczak, M. M.; Dryer, D. A.; Jacobson, D. D.; Foss, M. G.; Flynn, N. T. pH Dependent Redox Couple: An Illustration of the Nernst Equation. *J. Chem. Educ.* **1997**, *74* (10), 1195. DOI: 10.1021/ed074p1195.

(36) Hou, S.; Xu, L.; Mukherjee, S.; Zhou, J.; Song, K.-T.; Zhou, Z.; Zhang, S.; Ma, X.; Warnan, J.; Bandarenka, A. S.; et al. Impact of Organic Anions on Metal Hydroxide Oxygen Evolution Catalysts. *ACS Catal.* **2024**, 12074-12081. DOI: 10.1021/acscatal.4c01907.

(37) Dinca, M.; Surendranath, Y.; Nocera, D. G. Nickel-borate oxygen-evolving catalyst that functions under benign conditions. *Proc. Natl. Acad. Sci. U. S. A.* **2010**, *107* (23), 10337-10341. DOI: 10.1073/pnas.1001859107.

(38) Beranek, R. (Photo)electrochemical Methods for the Determination of the Band Edge Positions of TiO_2-Based Nanomaterials. *Adv. Phys. Chem.* **2011**, *2011* (1), 786759. DOI: 10.1155/2011/786759.

(39) Tombácz, E. pH-dependent surface charging of metal oxides. *Period. Polytech. Chem. Eng.* **2009**, *53* (2), 77–86. DOI: 10.3311/pp.ch.2009-2.08.

(40) Liu, L.; Tian, Y.; Yang, X.; Liu, C. Mechanistic Insights into Water Autoionization through Metadynamics Simulation Enhanced by Machine Learning. *Phys. Rev. Lett.* **2023**, *131* (15), 158001. DOI: 10.1103/PhysRevLett.131.158001.

(41) Wang, J.; Zhao, Y.; Setzler, B. P.; Rojas-Carbonell, S.; Ben Yehuda, C.; Amel, A.; Page, M.; Wang, L.; Hu, K.; Shi, L.; et al. Poly(aryl piperidinium) membranes and ionomers for hydroxide exchange membrane fuel cells. *Nat. Energy* **2019**, *4* (5), 392-398. DOI: 10.1038/s41560-019-0372-8.

(42) Mitchell, J. B.; Chen, L.; Langworthy, K.; Fabrizio, K.; Boettcher, S. W. Catalytic Proton–Hydroxide Recombination for Forward-Bias Bipolar Membranes. *ACS Energy Lett.* **2022**, *7* (11), 3967-3973. DOI: 10.1021/acsenergylett.2c02043.

(43) Kosmulski, M. Compilation of PZC and IEP of sparingly soluble metal oxides and hydroxides from literature. *Adv. Colloid Interface Sci.* **2009**, *152* (1-2), 14-25. DOI: 10.1016/j.cis.2009.08.003.
(44) Kosmulski, M. Isoelectric points and points of zero charge of metal (hydr)oxides: 50years after Parks' review. *Adv. Colloid Interface Sci.* **2016**, *238*, 1-61. DOI: 10.1016/j.cis.2016.10.005.
(45) Ding, X.; Scieszka, D.; Watzele, S.; Xue, S.; Garlyyev, B.; Haid, R. W.; Bandarenka, A. S. A Systematic Study of the Influence of Electrolyte Ions on the Electrode Activity. *ChemElectroChem* **2022**, *9* (1), e202101088. DOI: 10.1002/celc.202101088.
(46) Tan, S.; Feng, H.; Zheng, Q.; Cui, X.; Zhao, J.; Luo, Y.; Yang, J.; Wang, B.; Hou, J. G. Interfacial Hydrogen-Bonding Dynamics in Surface-Facilitated Dehydrogenation of Water on TiO_2(110). *J. Am. Chem. Soc.* **2020**, *142* (2), 826-834. DOI: 10.1021/jacs.9b09132.
(47) Li, S. C.; Chu, L. N.; Gong, X. Q.; Diebold, U. Hydrogen bonding controls the dynamics of catechol adsorbed on a TiO_2(110) surface. *Science* **2010**, *328* (5980), 882-884. DOI: 10.1126/science.1188328.

TOC Graphic

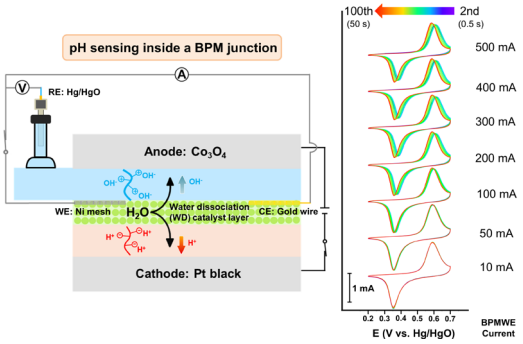
pH sensing inside a BPM junction
RE: Hg/HgO
Anode: Co_3O_4
WE: Ni mesh
H_2O
Water dissociation (WD) catalyst layer
CE: Gold wire
Cathode: Pt black
100th (50 s)
2nd (0.5 s)
500 mA
400 mA
300 mA
200 mA
100 mA
50 mA
10 mA
1 mA
0.2 0.3 0.4 0.5 0.6 0.7
E (V vs. Hg/HgO)
BPMWE Current